Journal of Applied Electrochemistry **34**: 643–651, 2004.

Application of combinatorial methodologies to the synthesis and characterization of electrolytic manganese dioxide

M. DEVENNEY[1], S.W. DONNE[2,3]* and S. GORER[1]
[1]*Symyx Technologies, Inc., 3100 Central Expressway, Santa Clara, CA 95051, USA*
[2]*Eveready Battery Company, Inc., 25225 Detroit Road, Westlake, OH 44145, USA*
[3]*Discipline of chemistry, University of Newcastle, Callaghan, NSW 2308, Australia*
*(*author for correspondence, e-mail: scott.donne@newcastle.edu.au)*

Received 9 October 2003; accepted in revised form 23 December 2003

Key words: batteries, battery materials, combinatorial methods, electrolytic manganese dioxide

Abstract

A combinatorial method has been used to investigate the effects of anodic current density, and Mn(II) and H_2SO_4 concentrations on the electrochemical synthesis and characterization of electrolytic manganese dioxide (EMD). The combinatorial method involved rapid parallel and series electrochemical deposition of EMD from electrolytes with various Mn(II) (0.15–1.82 M) and H_2SO_4 (0.05–0.51 M) concentrations, at various anodic current densities (25–100 A m^{-2}), onto individual 1 mm^2 titanium electrodes, in an overall array consisting of 64 electrodes. Electrode characterization was then by average plating voltage (recorded during deposition), and open circuit voltage and chronoamperometric discharge in 9 M KOH. The applicability and benefit of the method was demonstrated by identifying the conditions of 0.59 M Mn(II), 0.17 M H_2SO_4 and 62.5 A m^{-2} anodic current density as leading to the best performing EMD. These are comparable with existing knowledge regarding the synthesis and electrochemical performance of EMD, demonstrating clearly the capabilities of the combinatorial method, and providing a starting point for future experimentation. An added benefit of the method in this work was the considerable time saved during experimentation.

1. Introduction

1.1. *Batteries and battery materials*

The popularity of portable consumer electronic devices has increased considerably over the past 5–10 years, and with that the demand for suitable power sources, namely batteries, has also increased. The alkaline Zn/MnO_2 primary still is still popular, due mainly to the behaviour of the manganese dioxide cathode. It has the ability to operate effectively under both moderate and low rate discharge conditions, over a wide temperature range. It has the additional advantages of being environmentally benign, as well as relatively inexpensive to produce on a commercial scale. Despite these excellent characteristics, there is still an increasing demand for an improved alkaline manganese dioxide cathode. Using the manganese dioxide cathode as an example, the aim of this work is to describe a methodology by which the rate of product development can be enhanced.

Manganese dioxide exists in many different polymorphs, of which the γ-form has been shown to possess the highest electrochemical activity. The original structural model proposed by De Wolff [1] suggested that γ-MnO_2 was an intergrowth of pyrolusite (β-MnO_2) and ramsdellite. Based on this, Ruetschi et al. [2–4] included the concepts of cation vacancies and structural water. Chabre and Pannetier [5] refined this even further by introducing the concept of microtwinning. Subsequent structural work has focused on further clarification through the use of TEM, electron diffraction and Rietveld analysis [6–8]. What is apparent from all these studies is that γ-MnO_2 can possess a widely varying structural composition, and hence electrochemical activity [9]. With this inherent variation a link needs to be established between synthesis conditions, structural composition and electrochemical activity.

γ-MnO_2 is prepared typically using an electrolytic process (EMD) the details of which have been described elsewhere [10]. In short, the critical production step involves anodic deposition of EMD (current density of 20–100 A m^{-2}) onto a titanium substrate from a hot (90–99 °C), acidic (~0.3 M H_2SO_4) solution of $MnSO_4$ (~1.0 M). The combination of these synthesis conditions determines the structural composition of the resultant EMD [9]; however, their effect on EMD electrochemical activity has not been well characterized. To establish this relationship on a commercial, or even a laboratory scale would be a significant endeavour. Therefore, what is required is a rapid and reliable technique by which

samples of EMD can be prepared and evaluated electrochemically under controlled conditions, all within a reasonable timeframe.

1.2. *Combinatorial materials science and electrochemistry*

The combinatorial process involves application of high throughput synthesis and screening techniques giving researchers the ability to more rapidly discover and optimize new materials. The techniques are finding numerous applications in materials science and catalysis, enabling increased experimental throughput by up to several orders of magnitude [11, 12]. Combinatorial methodologies have also been applied in the field of electrochemistry.

Mallouk and coworkers [13] developed a rapid combinatorial synthesis and fluorescent screening method for the exploration of ternary and quaternary anode electrocatalysts for the direct methanol fuel cell (DMFC). The authors created libraries of alloys by using automated ink-jet deposition of metal salt precursors onto a conducting fibre paper, followed by reduction to form a metal deposit. After synthesis, the libraries were immersed in an electrolyte containing a fluorescent pH indicator. Screening was performed with a typical three electrode cell (electrode array as the working electrode) by conducting a single anodic potential sweep. The pH was known to drop in regions where methanol is being oxidized, and so the library was illuminated with UV light and observation of the highest fluorescent intensities was therefore used as an indicator of the catalytically most active spots.

Haushalter et al. [14] developed an alternative combinatorial approach to the rapid synthesis and screening of fuel cell electrocatalysts. Libraries of alloy materials were synthesized directly onto an 8×8 electrode array by combinatorial sputtering or parallel electroplating. Characterization involved parallel monitoring of the current–voltage–time behaviour of each individual electrocatalyst. The authors tested a number of catalytic concepts for the anodic electro-oxidation of methanol (DMFC), as well as the cathodic electro-reduction of oxygen in aqueous acidic electrolytes [15]. They demonstrated that for known systems the electrochemical activity, as measured directly on the thin film samples on the addressable electrochemical array, correlated with the activity of known powder samples.

1.3. *This work*

In this work, we have developed a combinatorial method for the synthesis and screening of EMD samples. The samples are rapidly synthesized under a range of experimental conditions, and then characterized electrochemically in a high-throughput screening apparatus, with the ultimate goal of linking synthesis conditions with electrochemical performance.

2. Experimental

2.1. *Electrode array preparation*

The basis for the array was a 7.5 cm diameter quartz disk (~0.1 cm thick), onto which an array of 64 titanium electrodes (each 1 mm^2), with their associated contact wires and contact points, was deposited using a combination of sputtering and UV photolithography (Figure 1).

Onto one side of the quartz disk, a layer of photo-resist material (3–5 μm thick) was applied by spin coating. The disk was then dried at ~105 °C for a few minutes. After cooling, a mask outlining the shape of the electrodes, contact wires and contact points was placed over the photo-resist coated side of the disk, which was then exposed to UV light curing the photo-resist, turning it into a solid resistive material, somewhat bonded to the quartz surface. The masked areas, unexposed to UV light, were removed from the disk by washing with xylene and then butyl acetate rinse. The disk was then dried under Ar at room temperature.

A thin layer (200–300 Å) of titanium was then sputtered onto the quartz disk, covering the entire surface. When complete, the disk was ultrasonicated in acetone to remove the cured photo-resist that was previously adhered to the quartz disk. This resulted in the removal of all titanium, except that deposited directly onto the quartz; i.e., the electrodes, contact wires and contact points. To ensure that only the electrodes and contact points were exposed, another photolithography step was carried out to cover the contact wires. This time, a mask covering only the electrodes and the contact points was used so that after curing (UV exposure) only they were exposed, with the remainder covered by cured photo-resist material.

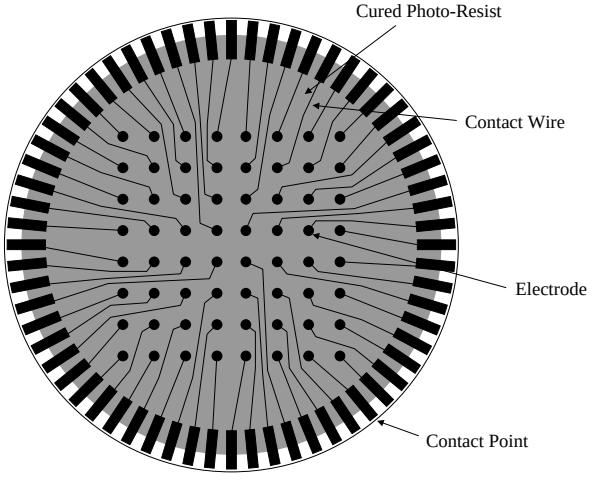

Fig. 1. Schematic diagram of the electrode array used in this work.

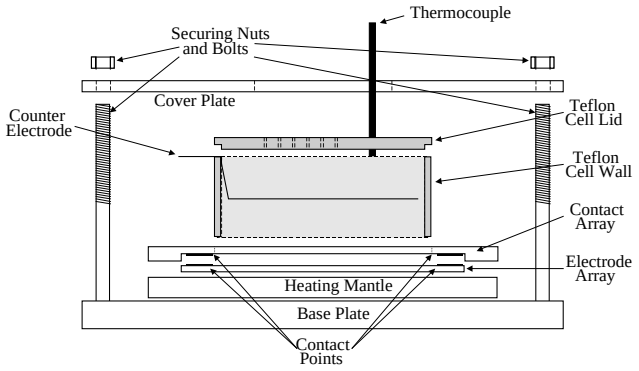

Fig. 2. Electrochemical cell used to deposit and electrochemically characterize EMD.

2.2. *EMD deposition*

A schematic of the electrochemical cell is shown in Figure 2. The cell bottom consists of the quartz disk mounted on a heating mantle, and held in place by an annular fixture, that also made independent contact to each electrode contact point on the disk. The cell wall was a Teflon tube mounted over the electrode array. A Pt counter electrode was placed in the cell above the electrode array, and its contact wire fed out over the cell wall. A Teflon lid was then placed over the cell to hold the counter electrode in place, and also to prevent evaporation during deposition. In the lid there were a number of holes used to either introduce electrolyte, other solutions to change the electrolyte composition, water and an Ar gas dispersion tube for stirring. A tube was also present to remove electrolyte from the cell. Another hole for thermocouple access was also provided. Addition and removal of solutions from the electrochemical cell was carried out by an automated pumping system to ensure speed and accuracy.

Once the appropriate electrolyte had been prepared in the cell, the heating mantle was turned on and the electrolyte allowed to heat up to the desired temperature, which was controlled via the thermocouple and a feedback loop to the mantle. While this was occurring, contact was made between each electrode and an individual working electrode input of an Arbin Instruments 64 channel potentiostat–galvanostat. The counter electrode, which also doubled as a pseudo-reference electrode, was made common for each channel. Once the electrolyte had reached the experimental temperature, EMD deposition was started on the appropriate electrodes. Once complete, and if further EMD deposition was to occur, the electrolyte could be changed by either adding another solution, or by pumping away the existing electrolyte, rinsing thoroughly with water and then adding the new electrolyte. Once the experimental temperature was again attained, deposition was continued. For each electrode, both the voltage and current were measured as a function of time. The deposition time was varied depending on the deposition current, so that the same amount of charge was used to deposit each EMD sample (2.1×10^{-3} C). Experience with the combinatorial technique indicated that if much more EMD was deposited, it would delaminate from the substrate during post-production treatment.

When EMD had been deposited on each electrode, the heating mantle was turned off and the cell rinsed thoroughly with water. Once clean, the electrode array was removed from the cell and dried in air at ~100 °C. Through experience it was found that EMD was deposited poorly at the edge of the electrode, exposing bare titanium. To overcome this, another layer of photo-resist material was applied to the electrode array, this time to cover the edge of each EMD electrode.

2.3. *EMD discharge performance*

Electrochemical characterization of each electrode was achieved using double-step chronoamperometry. The cell used for electrochemical discharge was similar to that used to synthesize the EMD (Figure 2). The only differences were the electrolyte, which for discharge was 9.0 M KOH, the presence of a Hg/HgO reference electrode, and the fact that the heating mantle was necessary only to support the electrode array. During discharge, the counter electrode (Pt wire) and reference electrode were common, while each EMD electrode was connected to an individual working electrode input of the Arbin potentiostat–galvanostat.

With the cell filled with electrolyte, the open circuit voltage (OCV) of each electrode was recorded for 20 s. Following this, the potential of each EMD electrode was stepped from the OCV to −0.4 V, where it was held for 240 s, and then immediately to −0.6 V for 60 s. During the voltage steps, the current was measured as a function of time.

3. Results and discussion

3.1. *EMD deposition*

The four key experimental parameters associated with EMD production are anodic current density, temperature, and Mn(II) and H_2SO_4 concentration. The ranges for these variables are wide, with anodic current densities ranging from 20 to 100 A m^{-2}, temperatures ranging from 90 to 99 °C, Mn(II) concentration limited only by $MnSO_4$ solubility, while the H_2SO_4 concentration lies in the range 0.05–0.6 M. These limits are determined mainly by the titanium anode substrate, which suffers from passivation at low temperatures, high current densities and high H_2SO_4 concentrations, and the preferred γ-MnO_2 structure, which is formed at all but low current densities. In this work, we investigated the applicability of the combinatorial method by synthesizing and characterizing a range of EMD samples under conditions of varying anodic current densities and Mn(II) and H_2SO_4 concentrations, as shown in Table 1. Because of its already very narrow experimental range, a

Table 1. Experimental conditions used for EMD deposition

Mn(II) /M	$[H_2SO_4]$ /M	Current density /A m^{-2}
0.18	0.51	100
0.59	0.40	100
1.00	0.28	100
1.41	0.17	100
1.82	0.05	100
0.18	0.40	81.3
0.59	0.28	81.3
1.00	0.17	81.3
1.41	0.05	81.3
0.18	0.28	62.5
0.59	0.17	62.5
1.00	0.05	62.5
0.18	0.17	43.8
0.59	0.05	43.8
0.18	0.05	25.0

constant temperature of 92 ± 1 °C was used. In an array consisting of 64 electrodes, the 15 conditions shown in Table 1 were repeated four times to evaluate the reproducibility of the technique.

A typical deposition voltage profile is shown in Figure 3. The plating voltage remains relatively constant during deposition, allowing the average plating voltage for each electrode to be calculated and used as an indicator of deposition behaviour. Figure 4(a) shows these average plating voltages as a function of the conditions under which they were prepared. It is clear that the average plating voltage increases as both the anodic current density and H_2SO_4 concentration increase. This result was expected given the predicted cell voltage based on the Nernst equation (Equation 1), and also from basic electrochemical kinetics which predict

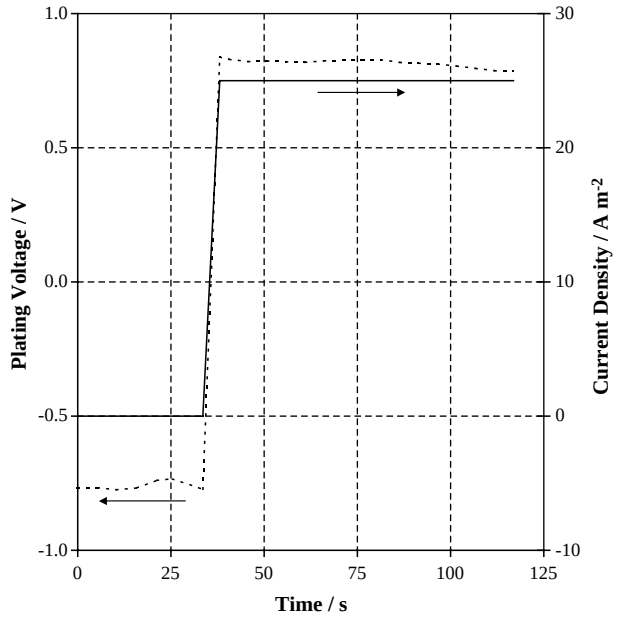

Fig. 3. Typical voltage profile, as a function of time, for EMD deposition.

that cell voltage increases with current density. Using the Nernst equation as a cell voltage predictor is the starting point for a future study into the kinetics of manganese dioxide deposition; however, comparing the experimental plating voltages with those predicted based on the electrolyte composition (Equation 1), as shown in Figure 5, indicates that the electrochemical kinetics for these reactions were sufficiently fast that there was little deviation from equilibrium. Deviations of the predicted data in Figure 5 probably arise from the use of concentrations instead of activities in the calculation, as well as variable H_2 partial pressures (1×10^{-6} atm was used here)

$$\begin{aligned}
&\text{Anode:} && Mn^{2+} + 2H_2O \leftrightarrow MnO_2 + 4H^+ + 2e^- \\
& && E^\circ = 1.280\,\text{V} \\
&\text{Cathode:} && 2H^+ + 2e^- \leftrightarrow H_2 \\
& && E^\circ = 0.000\,\text{V} \\
&\text{Overall:} && Mn^{2+} + 2H_2O \leftrightarrow MnO_2 + H_2 + 2H^+ \\
& && E_{\text{cell}} = E_{MnO_2/Mn^{2+}} - E_{H^+/H_2} \\
& && = 1.280 + \frac{RT}{2F}\ln\left(\frac{p_{H_2} \cdot a_{H^+}^2}{a_{Mn^{2+}}}\right)
\end{aligned} \tag{1}$$

From Equation 1 we can also predict that the plating cell voltage should increase as the Mn(II) concentration decreases. However, the experimental data in Figure 4(a) suggest that the Mn(II) concentration has little effect. This can perhaps be justified by noting that a factor of 10 decrease in the Mn(II) concentration will only increase the cell voltage by 0.036 V, which is almost indistinguishable from the variability in the plating voltage measurements, which on average was 3.9% (0.036 V), and at most 9.6% (0.089 V).

Typical commercial plating cells operate at ~2 V. However, these cells use cathodes of either graphite or copper which would be expected to increase the cell voltage, as would the build up of more resistive EMD on the anode, which would increase cell ohmic polarization.

So as to ensure consistency between the EMD produced in this work and that available commercially, an array was prepared in which the same EMD was deposited on each electrode (65 A m^{-2}, 1.0 M Mn(II), 0.28 M H_2SO_4 and 92 °C). The small amount of deposited EMD was then scraped off each electrode, ground into a powder, and examined by X-ray diffraction (XRD) (CuK_α radiation). Figure 6 shows that the XRD pattern of the array EMD was very similar to that of the commercial EMD sample (Eveready Battery Co., Inc.) recorded under the same conditions, the only significant difference being the ~22° 2θ peak for the array EMD being more diffuse. This can be accounted for by the fact that this peak is typically broad in the EMD XRD pattern, and the conditions under which the array EMD was prepared are slightly different compared to the commercial EMD. Nevertheless, the XRD

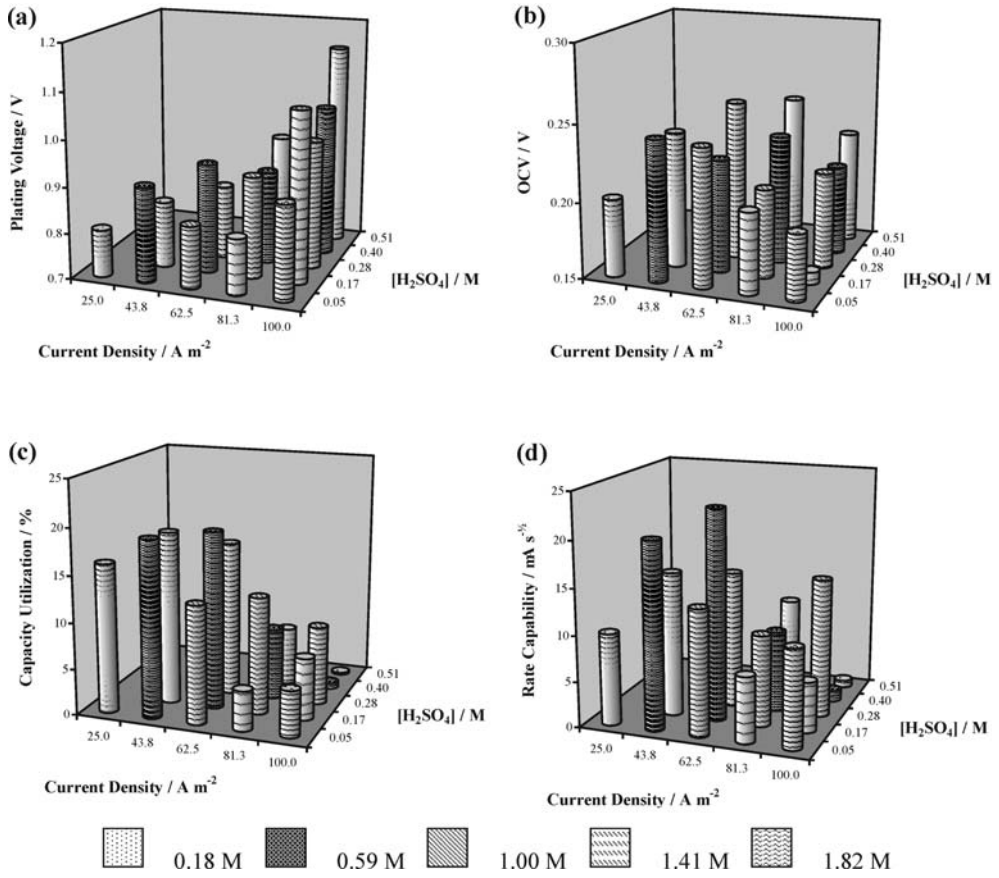

Fig. 4. Results as a function of $[H_2SO_4]$, [Mn(II)] and anodic current density: (a) average plating voltage; (b) open circuit voltage; (c) capacity utilization; and (d) rate capability.

pattern of the array EMD confirms that it is a similar material to commercially available EMD. This provided us with confidence that the following electrochemical characterization results would be representative of a large scale material.

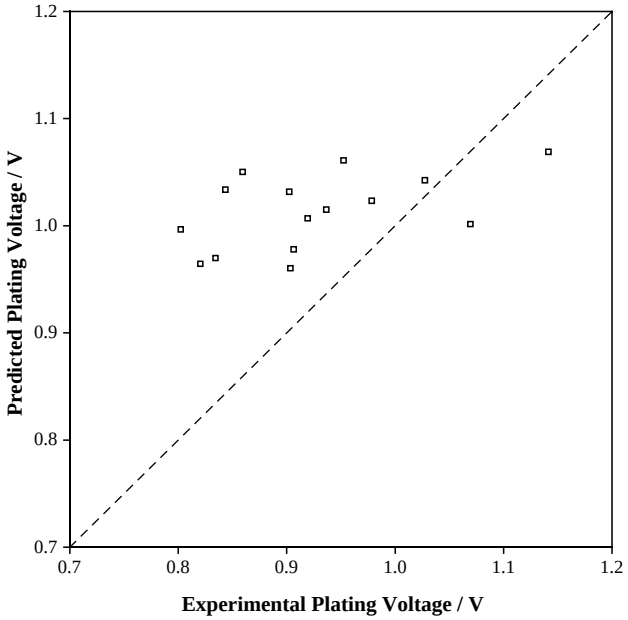

Fig. 5. Comparison between experimental and predicted plating voltages.

3.2. *Open circuit voltage*

After deposition the array was returned to the electrochemical cell, this time for discharge in 9 M KOH. The OCV is a measure of electrochemical potential, as well as being a reflection of EMD composition. The cation vacancy model proposed by Ruetschi et al. [2–4] suggests that the composition of EMD (γ-MnO_2) may be described by

$$(Mn^{4+})_{1-x-y} \cdot (Mn^{3+})_x \cdot (\square)_y \cdot (O^{2-})_{2-x-4y} \cdot (OH^-)_{x+4y} \quad (2)$$

in which $\square$ represents a cation vacancy, and that charge compensation in the presence of Mn^{3+} and cation vacancies is with protons (structural water). The OCV reflects the content of Mn^{4+} and cation vacancies; an increase in both causes the OCV to rise. Changes in EMD structural composition can also affect the OCV, since pyrolusite has a lower potential compared to ramsdellite. From a commercial standpoint, EMD should have a high Mn^{4+} content, so as to maximize the available capacity, and also increase the OCV.

The OCV for each EMD electrode in the array is shown in Figure 4(b). The data suggests that the OCV can be increased by lowering the concentration of

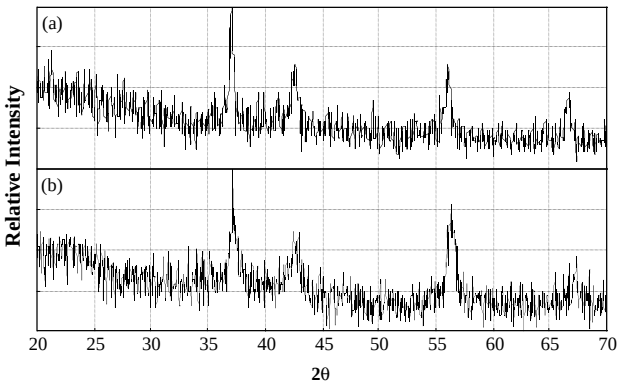

Fig. 6. XRD patterns (CuK_α radiation) of (a) EMD extracted from an array, and (b) commercial EMD.

Mn(II) and increasing the concentration of H_2SO_4. Increasing the anodic current density also increases the OCV, except when high Mn(II) and low H_2SO_4 concentrations are used.

From the EMD composition shown in Equation 2, we can predict an OCV increase with a higher Mn^{4+} content and also a higher relative proportion of less stable MnO_2 phases; i.e., ramsdellite and cation vacancies. During deposition it would seem logical that more Mn^{4+} and unstable MnO_2 phases would be formed in the EMD when deposition was carried out at a higher voltage. Therefore, those synthesis conditions that lead to a higher average plating voltage, should also lead to a sample with a higher OCV. Figure 7 compares the measured EMD OCV with average plating voltage and, contrary to expectations, there is not a strong relationship between EMD OCV and plating voltage. Therefore, there must be another overriding factor, perhaps relating to EMD structure, that influences the OCV.

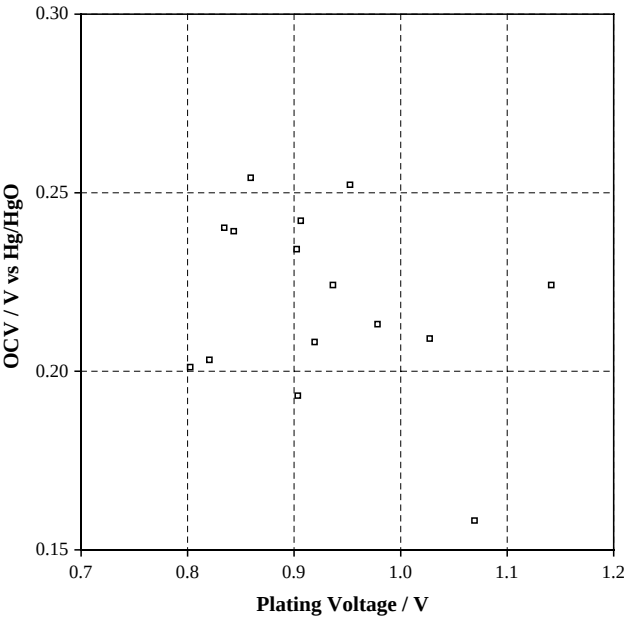

Fig. 7. OCV as a function of plating voltage for each of the EMD electrodes.

3.3. *EMD discharge*

The final stage in this work was to electrochemical characterise each EMD electrode. Discharge of EMD (γ-MnO_2) in concentrated alkaline electrolytes occurs via proton and electron insertion [16–20]. An electron from the external circuit is inserted into the EMD structure, reducing a Mn^{4+} ion to Mn^{3+}. For charge neutrality, a proton, originating from water decomposition at the EMD/electrolyte interface, is also inserted into the structure to form OH^-. At equilibrium both protons and electrons are distributed uniformly throughout the structure. The rate capability of an EMD can therefore be defined by how quickly protons and electrons can be transported throughout the EMD structure, ultimately heading towards a uniform distribution. This discharge can be represented by

$$(Mn^{4+})_{1-x-y}\cdot(Mn^{3+})_x\cdot(\square)_y\cdot(O^{2-})_{2-x-4y}\cdot(OH^-)_{x+4y} + \Delta H_2O + \Delta e^- \rightarrow (Mn^{4+})_{1-x-y-\Delta}\cdot(Mn^{3+})_{x+\Delta}\cdot(\square)_y \cdot(O^{2-})_{2-x-4y-\Delta}\cdot(OH^-)_{x+4y+\Delta} + \Delta OH^- \quad (3)$$

The voltage range over which solid state reduction occurs is from the OCV to −0.4 V vs Hg/HgO.

At lower voltages, the EMD electrode undergoes its 'second electron' reduction [16, 21]. Towards the end of solid state reduction, Mn^{3+} ions predominate within the EMD structure. This Mn(III) oxy-hydroxide is reasonably soluble in concentrated alkaline electrolytes [22], and after dissolution at sufficiently low potentials, the soluble Mn(III) species can be reduced on the surface of an electronic conductor to a Mn(II) species which precipitates almost immediately as $Mn(OH)_2$, due to the lower solubility of Mn(II) in concentrated alkaline electrolytes. While this second electron reduction provides additional discharge capacity, it is limited by its low efficiency (due to the very poor electronic conductivity of $Mn(OH)_2$) and low operating potential, meaning that it is unsuitable for emerging high power applications.

Many electrochemical methods have been used to characterize the electrochemical performance of EMD, including constant current discharge, voltammetry, step-potential electrochemical spectroscopy (SPECS) and electrochemical impedance spectroscopy (EIS). These techniques can provide a substantial amount of information related to EMD discharge; however, they tend to be relatively long term tests. Here, double-step chronoamperometry was chosen because (i) it is a relatively fast experiment suitable for combinatorial applications; (ii) it provides high rate discharge data for each EMD sample; (iii) it can also provide capacity utilization information; and (iv) it can characterize both the first and second electron reduction reactions. A typical discharge profile is shown in Figure 8.

3.3.1. *Capacity utilization*

The capacity utilization of an EMD electrode is defined as the capacity extracted a fixed time after the first

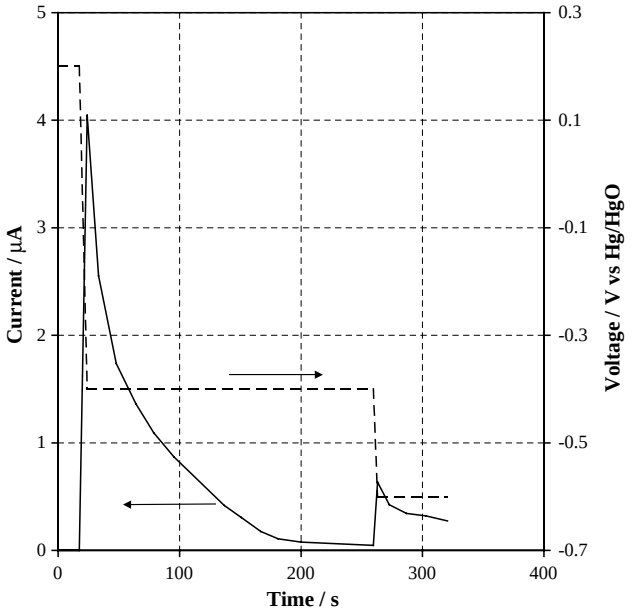

Fig. 8. Typical discharge profile for an array electrode.

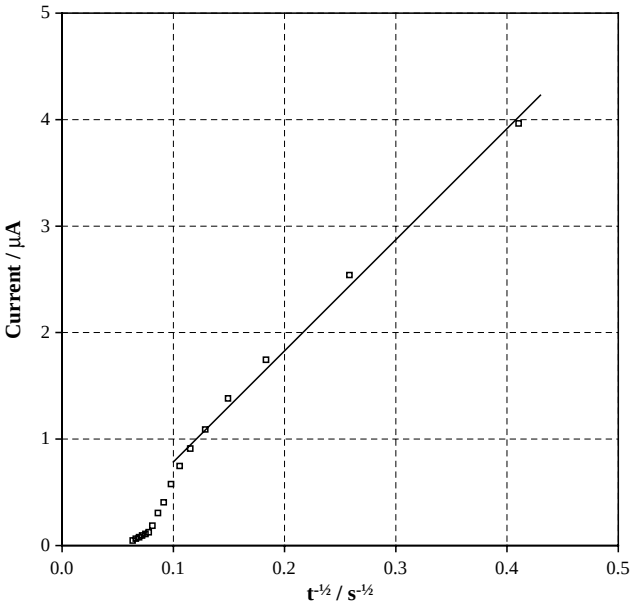

Fig. 9. Typical plot of cathodic current ($i(t)$) vs $t^{\frac{-1}{2}}$ for an EMD array electrode.

voltage step ($Q(t)$), compared to the total available capacity calculated from deposition data (Q_{Total}); i.e.,

$$\text{Capacity utilization } (\%) = \frac{Q(t)}{Q_{\text{Total}}} \times 100 \qquad (4)$$

$Q(t)$ was calculated by integration of the current vs time data during chronoamperometric discharge, while Q_{Total} was calculated from the deposition current. Figure 4(c) shows the capacity utilization of each array electrode 200 s after the onset of the first voltage step. This figure shows that the capacity utilization is most efficient in the range of experimental space bounded by 25.0–62.5 A m^{-2}, 0.05–0.28 M H_2SO_4 and 0.18–1.00 M Mn(II), with the most efficient EMD produced using 62.5 A m^{-2}, 0.17 M H_2SO_4 and 0.59 M Mn(II). The mechanistic reasons why these synthetic conditions lead to a superior EMD involves a complex interaction between soluble intermediates formed during deposition, the nature of the substrate and any competing reactions. Understanding this interaction, and how it influences the resultant structure of the EMD, will be the focus of future work. What is significant is that these synthetic conditions were identified reproducibly (average ~5% variability), and are in the range of commercial EMD synthesis conditions [9]. They also provide a starting point for further, more specific experimentation. This point emphasizes the importance and benefit of combinatorial methods; namely, identification of the preferred region of experimental space for more detailed follow up experimentation. Furthermore, in the absence of a combinatorial approach, covering the same broad region of experimental space would have required an estimated 4-fold increase in time.

3.3.2. *Rate capability*

Capacity utilization data provides an initial indication of which EMD samples possess enhanced rate capability, since a higher discharge current after the initial current step means that more charge will be passed in a set time. However, capacity utilization does not give a direct indication of rate capability, since the shape of the current vs time curve could change between electrodes, with the same amount of charge having been passed. To obtain a direct measure of rate capability, we have made use of the Cottrell equation for planar, semi-infinite diffusion during chronoamperometry [23]. The use of this expression is based on the assumption of planar diffusion away from the EMD surface, which on the microscopic scale is justified, and that diffusion is semi-infinite; i.e., diffusion planes within the EMD do not merge. This assumption can be justified at short times after applying the voltage step. Therefore, a plot of $i(t)$ vs $t^{-1/2}$ should be a straight line with a slope proportional to the diffusion coefficient. An absolute assessment of the diffusion coefficient is not possible since certain experimental values are not known accurately; e.g., the electrochemically active surface area. However, they are assumed constant for each electrode and so the slope of the $i(t)$ vs $t^{-1/2}$ plot can be used as a measure of rate capability.

A typical example is shown in Figure 9. The straight line in this figure shows the portion of the data used to determine the rate capability. At smaller values of $t^{-1/2}$ (larger t) the data deviate from linearity due to breakdown of the assumptions used in the Cottrell equation. A rate capability comparison for each of the array electrodes is shown in Figure 4(d). The trends in rate capability (as well as variability) are similar to that observed for capacity utilization, with a region of experimental space bounded by 25.0–62.5 A m^{-2},

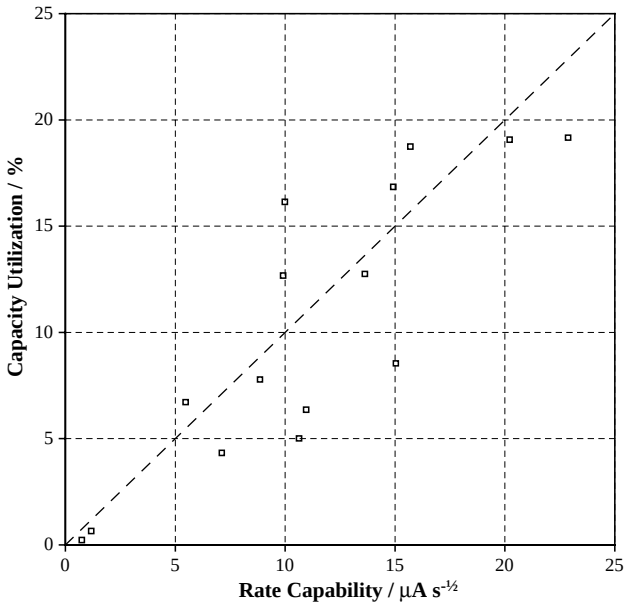

Fig. 10. Comparison between the rate capability and capacity utilization for each EMD array electrode.

0.05–0.28 M H_2SO_4 and 0.18–1.00 M Mn(II) exhibiting superior performance. Furthermore, the best performing material was produced at 62.5 A m^{-2}, 0.17 M H_2SO_4 and 0.59 M Mn(II). The similarity in behaviour between rate capability and capacity utilization can be confirmed by the comparison shown in Figure 10. For those EMD electrodes with similar capacity utilization, those that have a higher rate capability would be preferred. In general, for a fixed capacity utilization, the data points above the line in Figure 10 represent samples that can transport hydrogen much faster through the EMD structure than the corresponding samples below the line.

4. Summary and conclusions

We have developed a combinatorial method to assist in developing a relationship between EMD synthesis conditions and electrochemical performance. An array of 64 1 mm^2 titanium electrodes, with their associated leads and contact points, was prepared on a 7.5 cm diameter quartz disk, using a combination of radio frequency sputtering and UV photolithography. EMD was then deposited onto each of these electrodes using a range of experimental conditions; i.e., 0.15–1.82 M Mn(II), 0.05–0.51 M H_2SO_4, 25–100 A m^{-2} anodic current density, and a temperature of 92 °C. The average plating voltage during deposition was found to increase with both H_2SO_4 concentration and anodic current density. This is in agreement with commercial experience, as well as the trends predicted from electrochemical thermodynamics and kinetics.

Each EMD electrode in the array was characterized electrochemically in terms of its OCV and its capacity utilization and rate capability from chronoamperometric discharge. With some exceptions, the OCV increased when a higher H_2SO_4 and lower Mn(II) concentration were used, as well as a higher anodic current density. The OCV can be used as a measure of both chemical and structural composition, with more Mn^{4+}, cation vacancies and ramsdellite in the γ-MnO_2 expected to increase the OCV. Despite the similarities in behaviour between average plating voltage and OCV, the correlation between these two results is not clear.

Electrochemical characterization was by chronoamperometry, from which capacity utilization and rate capability data were extracted. Both of these characterization methods identified the synthetic variable ranges 25.0–62.5 A m^{-2}, 0.05–0.28 M H_2SO_4 and 0.18–1.00 M Mn(II) as giving a superior material, with the conditions of 62.5 A m^{-2}, 0.17 M H_2SO_4 and 0.59 M Mn(II) leading to the best performing EMD. While these ranges are broad, they do encompass commercial synthetic conditions, as well as providing a starting point for further, more detailed, experimentation.

In conclusion, this work has shown that combinatorial methods can be applied reliably to the production and characterization of EMD. The method led to results comparable with existing synthesis parameters for commercial EMD production, as well as provided a range of parameter values for further study, all within a substantially reduced timeframe.

References

1. P.M. De Wolff, *Acta Cryst.* **12** (1959) 341.
2. P. Ruetschi, *J. Electrochem. Soc.* **131** (1984) 2737.
3. P. Ruetschi, *J. Electrochem. Soc.* **135** (1988) 2657.
4. P. Ruetschi and R. Giovanoli, *J. Electrochem. Soc.* **135** (1988) 2663.
5. Y. Chabre and J. Pannetier, *Prog. Solid State Chem.* **23** (1985) 1.
6. A.H. Heuer, A. He, P.J. Hughes and F.H. Feddrix, *ITE Lett.* **1** (2000) B50.
7. W. Bowden, R. Sirotina and S. Hackney, *ITE Lett.* **1** (2000) B27.
8. D.E. Simon, T.N. Anderson and C.D.F. Elliott, *ITE Lett.* **1** (2000) B1.
9. R.P. Williams, R. Fredlein, G. Lawrance, D. Swinkels and C. Ward, *Prog. Batteries Battery Mater.* **13** (1993) 102.
10. C.B. Ward, A.I. Walker and A.R. Taylor, *Prog. Batteries Battery Mater.* **11** (1992) 40.
11. B. Archibald, O. Brummer, M. Devenney, D.M. Giaquinta, B. Jandeleit, W.H. Weinberg and T. Weskamp, *in* K.C. Nicolaou, R. Hanko and W. Hartwig (Eds). 'Handbook of Combinatorial Chemistry' (Wiley-VCH, 2002) p. 1017.
12. B. Archibald, O. Brummer, M. Devenney, S. Gorer, B. Jandeleit, T. Uno, W.H. Weinberg and T. Weskamp, *in* K.C. Nicolaou, R. Hanko and W. Hartwig (eds). 'Handbook of Combinatorial Chemistry' (Wiley-VCH, 2002) p. 885.
13. E. Reddington, A. Sapienza, B. Gurau, R. Viswanathan, S. Sarangapani, E.S. Smotkin and T. Mallouk, *Science* **280** (1998) 1735.
14. R.C. Haushalter, L. Matsiev and C.J. Warren, U.S. Patent 6,187,164, 2001.
15. P. Strasser, S. Gorer and M. Devenney, *in* 'Proceedings of the International Symposium on Fuel Cells for Electric Vehicles, 41st Battery Symposium', Nagoya, Japan, 2000, p. 153.
16. A. Kozawa and J.F. Yeager, *J. Electrochem. Soc.* **112** (1965) 959.

17. A. Kozawa and R.A. Powers, *J. Electrochem. Soc.* **113** (1966) 870.
18. S.W. Donne, G.A. Lawrance and D.A.J. Swinkels, *J. Electrochem. Soc.* **144** (1997) 2949.
19. S.W. Donne, G.A. Lawrance and D.A.J. Swinkels, *J. Electrochem. Soc.* **144** (1997) 2954.
20. S.W. Donne, G.A. Lawrance and D.A.J. Swinkels, *J. Electrochem. Soc.* **144** (1997) 2961.
21. A. Kozawa and J.F. Yeager, *J. Electrochem. Soc.* **115** (1968) 1003.
22. A. Kozawa, T. Kalnoki-Kis and J.F. Yeager, *J. Electrochem. Soc.* **113** (1966) 405.
23. A.J. Bard and L.R. Faulkner, 'Electrochemical Methods – Fundamentals and Applications', 2nd edn (John Wiley and Sons, 2001).